

The annual and longitudinal variations in plasmaspheric ion density

F. W. Menk,¹ S. T. Ables,¹ R. S. Grew,¹ M. A. Clilverd,² and B. R. Sandel³

Received 12 August 2011; revised 17 December 2011; accepted 22 December 2011; published 13 March 2012.

[1] This paper shows that at solar maximum, equatorial ion densities at $L = 2.5$ are substantially higher at American longitudes in the December months than in the June months. This arises because the configuration of the geomagnetic field causes a longitude-dependent asymmetry in ionospheric solar illumination at conjugate points that is greatest at American longitudes. For example, at -60°E geographic longitude the $L = 2.5$ field line has its foot point near 65° geographic latitude in the Southern Hemisphere but near 42° latitude in the Northern Hemisphere. We investigated the consequent effects on equatorial electron and ion densities by comparing ground-based observations of ULF field line eigenoscillations with in situ measurements of electron densities (from the CRRES and IMAGE spacecraft) and He^+ densities (IMAGE) for $L = 2.5$ at solar maximum. Near -60°E longitude the electron and ion mass densities are about 1.5 and 2.2 times larger, respectively, in the December months than in the June months. Over the Asia-Pacific region there is little difference between summer and winter densities. Plasmaspheric empirical density models should be modified accordingly. By comparing the electron, helium, and mass densities, we estimate the annual variation in H^+ , He^+ , and O^+ concentrations near -3°E longitude and -74°E longitude. In each case the He^+ concentration is about 5% by number, but O^+ concentrations are substantially higher at -3°E longitude compared with -74°E . We speculate that this may be related to enhanced ionospheric temperatures associated with the South Atlantic anomaly.

Citation: Menk, F. W., S. T. Ables, R. S. Grew, M. A. Clilverd, and B. R. Sandel (2012), The annual and longitudinal variations in plasmaspheric ion density, *J. Geophys. Res.*, 117, A03215, doi:10.1029/2011JA017071.

1. Introduction

[2] The purpose of this paper is to characterize how the electron and mass density and ion concentrations (H^+ , He^+ , O^+) near the equatorial region of the plasmasphere vary with time of year and geographic longitude at solar maximum. This study extends the work by Clilverd *et al.* [2007] who used Combined Release and Radiation Effects Satellite (CRRES) data to describe in detail the annual and longitudinal variations in plasmaspheric electron density, comparing these also with the variations in He^+ density measured with the IMAGE spacecraft EUV experiment [Sandel *et al.*, 2001].

[3] It has long been known that the electron density of the ionospheric F_2 region is unusually high in the December months compared with the June months [e.g., Berkner and Wells, 1938; Seaton and Berkner, 1939; Tremellen and Cox, 1947; Yonezawa and Arima, 1959]. This is called an

annual variation because it has the same phase in both hemispheres, in contrast to separate seasonal effects [e.g., Yonezawa, 1971; Torr and Torr, 1973], and its amplitude exceeds the 7% annual change in solar flux arising from the eccentricity of the Earth's orbit. A detailed discussion of this annual variation was presented by Rishbeth and Müller-Wodarg [2006]. The other important variations are a seasonal anomaly, in which daytime F_2 layer electron density peaks in winter, and a semiannual anomaly, in which density is greater at equinox than at solstice. The phasing of the annual (December maximum) and seasonal (winter maximum) variations also leads to a hemispheric asymmetry in F_2 region electron density [e.g., Torr and Torr, 1973; Zou *et al.*, 2000].

[4] The annual variation is also evident in topside electron density [King *et al.*, 1968; Su *et al.*, 1998] as well as in height-integrated total electron content (TEC) [e.g., Titheridge and Buonsanto, 1983]. By comparing GPS data for both hemispheres, Mendillo *et al.* [2005] showed that the global December–June asymmetry in TEC varies with longitude and is largest (a difference of the order of 60%) near -70°E (i.e., 70°W) longitude, where the differences between geographic and geomagnetic latitudes are greatest. The existence of a similar but smaller variation in neutral O/N_2 concentration led them to conclude that the TEC

¹School of Mathematical and Physical Sciences, University of Newcastle, Newcastle, New South Wales, Australia.

²British Antarctic Survey, Cambridge, UK.

³Lunar and Planetary Laboratory, University of Arizona, Tucson, Arizona, USA.

asymmetry is connected with global variations in thermospheric composition.

[5] The plasmasphere is dynamically linked to the underlying ionosphere, and the equatorial plasmaspheric electron density determined using natural VLF whistler signals exhibits a similar annual variation to that seen in the ionosphere [e.g., *Smith*, 1961; *Carpenter*, 1962]. *Park et al.* [1978] found that the December/June ratio in plasmaspheric electron density was about 1.5 at $L = 2.5$ at Eights, Antarctica (-77°E) during solar maximum, although *Tarcsai et al.* [1988] found no significant annual variation at $L = 2.5$ in Hungary (18°E) during solar minimum.

[6] *Clilverd et al.* [1991] studied the annual variation at solar minimum using a VLF Doppler experiment that detected artificially produced VLF signals that propagated mostly at nighttime along $L = 2.5$ flux tubes to Faraday, Antarctica (-64° geographic E). Electron densities in December were about three times higher than in June. (Note that the group delays shown for Dunedin by *Clilverd et al.* [1991, Figure 6] are actually for $L = 2.2$ but the densities on the right-hand axis relate to $L = 2.5$ and so should be rescaled accordingly. This does not affect the overall result or the present discussion.) By comparison with the variation in peak F_2 region electron density and using an empirical diffusive equilibrium model, *Clilverd et al.* deduced that at $L = 2.5$ the annual asymmetry should be much reduced at 180°E and almost nonexistent at 50°E . They attributed this annual variation to enhanced production and vertical transport of ionization (because of the action of neutral winds) in local summer at locations where the geographic (geomagnetic) latitudes are simultaneously relatively high (low).

[7] The most detailed observational study of the annual and longitudinal variations in plasmaspheric electron density is due to *Clilverd et al.* [2007]. They determined the density in situ with CRRES from July 1990 to October 1991, during solar maximum, and obtained the variation between December and June values as a function of longitude at different L values. The maximum variation was a factor of 2.5 at $L = 2.5$ near -60°E longitude. Charge neutrality suggests that plasmaspheric ion density should also exhibit annual and longitudinal variations. Accordingly, they also reported a similar form of variation in the equatorial He^+ abundance determined with the IMAGE EUV experiment described by *Sandel et al.* [2001].

[8] The mass density in the equatorial plane may be determined from measurements of field line resonance frequencies with ground-based magnetometers [e.g., *Menk et al.*, 1999; 2004]. Using data from a pair of magnetometers centered on $L = 1.74$, *Berube et al.* [2003] thus found that ion densities in December were 2–3 times higher than in June. However, at such low L shells, the field line resonance frequencies will be strongly influenced by O^+ mass loading in the underlying ionosphere, which modifies the Alfvén speed profile [*Hattingh and Sutcliffe*, 1987; *Waters et al.*, 1994]. Looking at field line resonance data recorded in July 1984 at three $L = 1.78$ stations spanning 35° in longitude, *Sutcliffe et al.* [1987] found that frequencies at -10°E were higher (and hence mass density lower) than at 20°E and 25°E . This agrees with the form of annual variation reported by *Clilverd et al.* [2007], who also compared their $L = 2.5$ electron density observations with mass density data, but only at two points in longitude.

[9] Extensive modeling effort has focused on the cause of the annual variation. *Güter et al.* [1995] suggested, using a numerical coupled ionosphere-thermosphere model, that at solar minimum and $L = 2$ the annual variation in plasmaspheric density is controlled by similar variations in ionospheric O^+ density in the Northern Hemisphere, although they were not able to reproduce the magnitude of the observed variation. The time-dependent model described by *Bailey and Sellek* [1990] and *Bailey et al.* [1997] incorporates an eccentric dipole geomagnetic field and $\mathbf{E} \times \mathbf{B}$ neutral meridional drifts and may explain observed plasmaspheric electron densities in July near $L = 2.5$ at American longitudes [*Rippeth et al.*, 1991]. The model has also been used to show that meridional neutral winds as well as thermospheric composition changes are required to account for annual variations in the topside electron density [*Su et al.*, 1998; *Kawamura et al.*, 2002]. An extensive analysis of the cause of the annual variation in plasmaspheric density was presented by *Richards et al.* [2000]. They assimilated measured as well as IRI ionosphere N_mF_2 and h_mF_2 into the model to avoid the wind ambiguity and found that the seasonal variation of the plasmaspheric plasma temperatures played the most important role in the annual plasmaspheric density variation.

[10] This paper has three main objectives. First, we extend the study by *Clilverd et al.* [2007] by analyzing electron and He^+ density data, both from the IMAGE spacecraft. *Clilverd et al.* compared CRRES electron density data from July 1990 to October 1991 with IMAGE data, mostly from 2001. We use different selection criteria and do not mix data from different solar cycles. Second, using ground magnetometers, we determine the variation in plasmaspheric mass density with longitude and season and compare this with the electron and He^+ density variations. Finally, following the work by *Grew et al.* [2007], we estimate the H^+ , He^+ , and O^+ concentrations and examine how these change with longitude and season. We find that for the 2001 solar maximum, electron and mass densities at $L = 2.5$ were about 1.5 and 2.2 times larger, respectively, in the December months than in the June months near -60°E geographic longitude (i.e., over the American sector). There was little difference between summer and winter densities over the entire Asia-Pacific sector spanning 50°E to -150°E longitude. Our electron density results are similar to (but slightly different from) those of *Clilverd et al.* [2007], but the mass density and ion concentration results are new.

2. Data Sources and Analysis

2.1. Electron Number Densities

[11] *Clilverd et al.* [2007] used electron density data based on the electron plasma frequency determined from CRRES spacecraft measurements for October to February, inclusive, and April to August, inclusive, representing the December and June solstices, respectively, over the 1990–1991 satellite life span. Electron densities were averaged for each season into 5° wide bins in geographic longitude for periods when the spacecraft was within $\pm 10^\circ$ of the magnetic equator. An amplitude threshold was used to ensure that only emissions from inside the plasmasphere were considered.

[12] The present study references these CRRES observations but is mostly based on electron densities from the

Radio Plasma Imager (RPI) experiment [Reinisch et al., 2001] on board the IMAGE spacecraft [Burch, 2003], which was in an elliptical polar orbit with apogee at $7.2 R_E$ (46,000 km), perigee at 1000 km altitude, and 14.2 h orbital period. The RPI instrument is a low-power radar that alternates between active and passive modes and spans the plasma resonance frequencies characteristic of the magnetosphere (3 kHz–3 MHz). In active mode, the electron cyclotron frequency is determined to within $\sim 0.1\%$ and the electron plasma frequency to within $\sim 1\%$ from stimulated plasma resonances and the Z and X mode wave cutoffs [Benson et al., 2003]. When operating in the passive mode, the RPI receives natural plasma wave emissions from 3 kHz to 1.1 MHz. The electron number density can then be determined to within a few percent from the upper hybrid emission band [Benson et al., 2004] or from the lower edge of a range of continuum radiation [e.g., Goldstein et al., 2003].

[13] We used the IMAGE-RPI electron density database (which is due to Y. Wang and P. Webb) available from the Virtual Wave Observatory web site (<http://vwo.gsfc.nasa.gov>), derived with an automatic algorithm using rules determined by the comparison of active and passive RPI data [Benson et al., 2004]. Following Clilverd et al. [2007] we compared electron densities for April–August, inclusive (“June months”), and October–February, inclusive (“December months”), for RPI measurements that simultaneously (i) were within $\pm 30^\circ$ of the magnetic equator, (ii) were between 07 and 16 MLT, (iii) were in the range $2.0 < L < 3.0$, and (iv) occurred only for $Kp \leq 4$ at that time and during the previous day. For (i) we assumed that electron density is constant along field lines over this 30° range; following the work of Vellante and Förster [2006], this assumption should introduce $< 10\%$ error under solar maximum conditions. Criterion (ii) ensures that electron densities are considered over the same range of local times as mass densities, as described below. Regarding (iii), we scaled electron densities to an equivalent value at $L = 2.5$ by assuming that densities vary across this range of L as L^{-4} . This is consistent with the variation in flux tube volume and previous observations [e.g., Chappell et al., 1970; Carpenter and Park, 1973; Park et al., 1978; Clilverd et al., 2007]. Finally, condition (iv) attempts to restrict the data set to the plasmasphere by excluding intervals associated with inward erosion of the plasmopause and other storm-related effects. Alternatively, given the Kp dependence in plasmopause position [e.g., Carpenter and Anderson, 1992] and the likely flux tube refilling time after severe storms, it was perhaps appropriate to exclude data when Kp reached 6 or greater in the preceding 8 days. Using our $Kp \leq 4$ approach, it was also necessary to exclude a small number of outlier points representing anomalously high or low densities.

[14] The resultant database comprised about 1480 June and 600 December electron density values, mostly from 2001, because of the IMAGE orbital configuration.

2.2. Determination of Plasmaspheric He^+ Density

[15] The He^+ ion density measurements presented in this study are the same as those used by Clilverd et al. [2007] and were obtained with the IMAGE spacecraft EUV experiment from line of sight measurements of the intensity of

resonantly scattered sunlight at 30.4 nm [Sandel et al., 2001].

[16] These He^+ data are based on 122 images from 15–17 June 2001 and 97 images from 9–20 December 2001. All images were from quiet times ($Kp \leq 2$) and chosen to avoid azimuthal structures that often appear during more active times. After transforming each image to the plane of the magnetic equator [Sandel et al., 2003] using magnetic longitude as the azimuthal coordinate, the images were summed to form a single image for each of June and December (omitting the region of Earth’s shadow and overlaps between the EUV cameras). Azimuthal profiles of brightness versus magnetic longitude were then obtained by sampling these composite images in an annulus of width $0.3 L$ centered at $L = 2.5$ with a bin size of 5° in magnetic longitude. As outlined by Clilverd et al. [2007], imperfect averaging of the diurnal variation in ion density does not significantly bias the structure measured in longitude. Equatorial He^+ abundances were inferred from the measured brightness using the concept of effective path length described by Clilverd et al. [2003] and Gallagher et al. [2005].

[17] The error in these He^+ densities depends on three factors: the uncertainty in absolute sensitivity (of the order of 20%), uncertainty arising from the counting statistics (very small when using summed images, as here), and the uncertainty in inferring local abundance from column abundance, which is significant but depends somewhat on the situation. The resultant overall error in He^+ abundance is conservatively estimated at 50% but would be lower when comparing one EUV measurement with another.

[18] In section 3.2 we compare model June and December He^+ density profiles obtained by averaging densities over 10° wide bins of longitude and determining polynomial fits. We also examine case studies in which He^+ densities averaged over 15° for a selected event longitude are compared with ion mass densities and electron number densities.

2.3. Determination of Plasmaspheric Mass Densities

[19] The ion mass densities presented in this study were calculated from field line resonant (FLR) frequencies measured with ground-based magnetometers, following the analytical expressions described by Taylor and Walker [1984] and Walker et al. [1992] and techniques summarized by Menk et al. [1999, 2000]. We used data from as many magnetometer stations (with at least 5 s timing cadence) as we could access near $L = 2.5$ for June and December 2001. Station details are given in Table 1, and locations are shown in Figure 1. For pairs of magnetometers that are closely spaced in latitude, the resonant frequency is identified by the peak in the H component cross power and cross phase and a unity crossing in the H component power ratio, approximately midway between the stations. Where only one station is available, the resonance is indicated by a peak in the H/D power ratio [e.g., Vellante et al., 1993] and a rapid change in polarization, i.e., in the phase between the H and D components.

[20] Resonant frequencies were independently determined using two completely separate approaches. First, cross-power and cross-phase spectra were visually examined for all days with $Kp \leq 4$ and all available stations for June and December 2001, and the resonant frequency was manually identified for each hour between 07:00 and 16:00 LT and

Table 1. Ground Magnetometer Stations Used for Determining Eigenfrequencies

Name	Code	Geographic Longitude (°E)	L Shell	Provider
Belsk	BEL	20.8	2.24	PAS
Crozet	CZT	51.9	2.84	EOST
Kataning	KAT	117.6	2.12	CPMN
Adelaide	ADL	138.7	2.10	CPMN
Launceston	LAU	147.1	2.71	UNC
Hobart	HBT	147.2	2.89	IPS
Magadan	MGD	150.9	2.92	CPMN
Paratunka	PTK	158.3	2.15	CPMN
Victoria	VIC	-123.4	2.92	CANMOS
Applied Phys Lab	APL	-76.9	2.46	MEASURE
Millstone Hill	MSH	-71.5	2.77	MEASURE
Escudero	ESC	-58.9	2.18	SAMBA
O'Higgins	OHI	-57.9	2.28	SAMBA
St John's	STJ	-52.3	2.90	CANMOS
Hartland	HAD	-4.5	2.25	SAMNET
York	YOR	-1.1	2.56	SAMNET

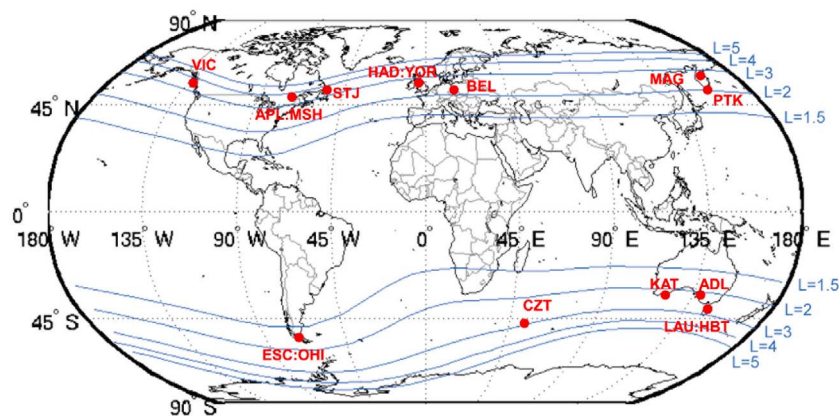
then averaged to produce daily and mean monthly values for each longitude sector. The above local times relate to when FLR frequencies are most frequently recorded, but not immediately near dawn when frequencies change rapidly because of rapid changes in O^+ scale height [e.g., *Kutiev et al.*, 2006]. This process was actually done twice, once by inspection of individual cross-phase or power ratio spectra [e.g., *Menk et al.*, 2006, Figure 3b] for each hour and each day, then separately by manually scaling values each hour from whole-day dynamic cross-phase and power ratio spectra.

[21] In order to ensure consistency across the data set by eliminating, as far as possible, subjective human intervention in analyzing spectra, the entire data set was then reexamined using automated algorithms to determine the resonant frequencies. Following the work by *Ables and Fraser* [2005], individual whole-day spectra were generated using a 256-point fast Fourier transform (FFT) with 50% overlap and using a pure state filter to determine spectral estimates and the degree of polarization for each estimate. Depending on availability, data for each station or

station pair spanning up to 30 contiguous days for each of June and December 2001 were averaged to produce whole-day spectra for both seasons. Using these averaged spectra, FLR frequencies were then determined using detection criteria that were hard-wired into the code for the two techniques used. The resultant FLR frequency estimates over each hour between 8:00 and 16:00 magnetic local time (MLT) were then taken as a statistical ensemble from which means were calculated and one standard deviation error ranges determined.

[22] Two different algorithms were used depending on whether data were available from single stations or from closely spaced station pairs. Where only single-station data were available, for each station, season-averaged power spectra of the H/D ratio were generated, with equal weight given to all spectral estimates. FLR frequency estimates for each hour in the averaged spectra were set to the frequency bin between 10 and 50 mHz, which had the maximum H/D ratio. Where closely spaced station pairs were available, cross-phase spectra were generated for the H components for each day and each pair, then averaged over each season. A masking process was applied in which spectral estimates that had a degree of polarization below 70% were not included in the estimates. The FLR frequency estimates for each time block in the averaged spectra were set to the frequency bin between 10 and 50 mHz, which had the peak cross phase (for which the reference station was nearest the geomagnetic equator). Figure 2 shows examples of this technique for the HAD:YOR and APL:MSH station pairs (United Kingdom and eastern U.S. sectors, respectively) for June and December. In each case, red dots identify the mean FLR frequency for each time bin, while the thick horizontal lines denote the monthly average over 8:00–16:00 MLT. Note that in this method the cross-phase spectra are actually quasi-ellipticity plots (in which the H component of the second station is taken as the y coordinate), since using the minimum in ellipticity produces no effective difference in the selected frequency (compared with cross-phase spectra) but in the averaging process results in a tighter range for the final estimates.

[23] In order to increase the number of available station pairs, the ADL:PTK interhemispheric pair was also used. *Pilipenko et al.* [1999] described the use of a “quasi-gradient”

**Figure 1.** Map in geographic coordinates showing magnetometer stations used in this study and L shell contour foot points.

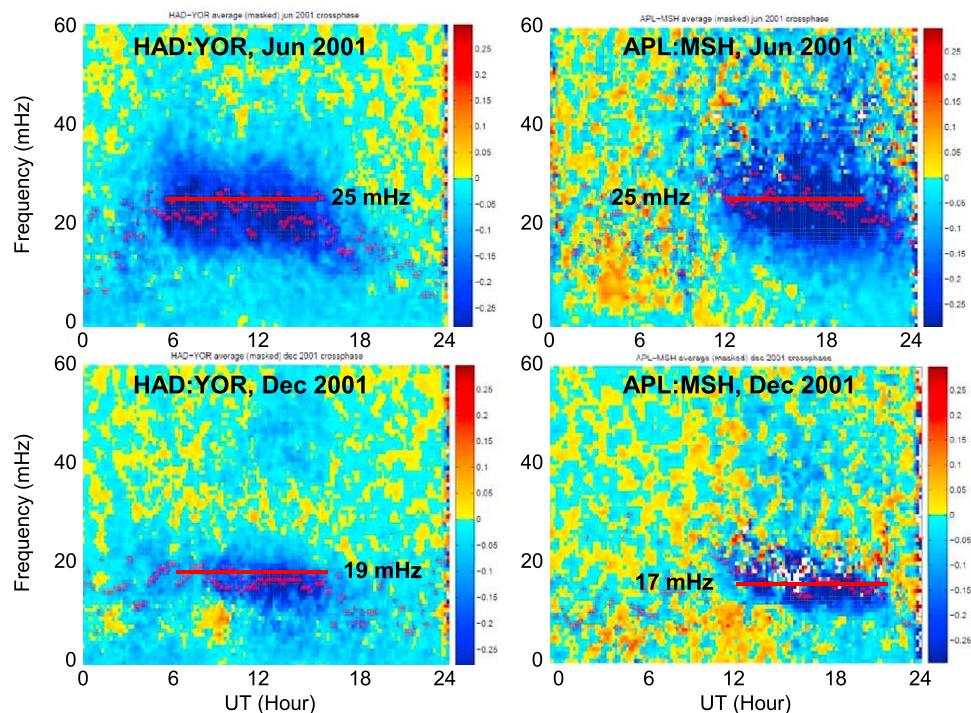


Figure 2. Example of monthly averaged FLR spectra for (left) HAD:YOR and (right) APL:MSH station pairs for (top) June and (bottom) December. Red dots denote mean FLR frequency for each time bin, and thick horizontal lines represent the monthly average over 8:00–16:00 MLT.

method, comparing the ratio of spectral densities, phase difference, and coherency between nearly conjugate stations, but this approach has otherwise not been widely reported.

[24] The results of these independent manual and algorithm-based approaches were compared and largely agreed within observational uncertainty. Results presented here are the means from these independent examinations.

[25] Mass densities at each available longitude were calculated from the frequency estimates using the approach described by *Menk et al.* [1999], assuming a dipole geomagnetic field and an r^{-3} dependence of density along the field line, where r is the radial distance from the Earth. Under quiet geomagnetic conditions, such densities are negligibly different from those obtained by solution of the toroidal magnetohydrodynamic (MHD) standing wave equation using the Tsyganeko 2001 empirical field model [Berube et al., 2006]. Mass densities were scaled to an equivalent value at $L = 2.5$ by assuming that densities vary with L as L^{-4} [e.g., Denton et al., 2009, and references discussed therein]. The uncertainty in the calculated mass densities thus depends mainly on one standard deviation uncertainty in the frequency measurement mentioned above.

2.4. Estimating Ion Concentrations

[26] By comparing estimates of the FLR-derived mass density M with RPI measurements of the electron number density N_e and EUV-based measurements of He^+ number density, it is possible to determine the relative heavy ion concentrations [Grew et al., 2007]. For a neutral plasma comprising $N = N_e$ electrons, x protons, y He^+ ions, and z O^+ ions, we have $N = x + y + z$ and M (amu cm^{-3}) = $x + 4y + 16z$, allowing the H^+ and O^+ concentrations to be

immediately found. This was done for June and December 2001 using the monthly average values obtained as outlined above for $L = 2.5$ and at -74°E and -3°E geographic longitudes, representing the eastern U.S. and UK sectors, respectively. Uncertainty in these estimates is of the order of 30%–50%.

3. Results

3.1. Variation in Electron Number Density

[27] The variations in electron number density with geographic longitude are shown in Figure 3 for the June and December months, based on RPI and CRRES observations, as outlined in section 2.1. The RPI data are from 2001 while the CRRES observations, previously presented by *Clilverd et al.* [2007], are from 1990–1991. The error bars represent one standard deviation in electron density, averaged over 20° bins (RPI data) and 5° bins (CRRES) in longitude.

[28] It is clear that the electron densities in both the RPI and CRRES data sets are much higher in the December than in the June months over the longitude range from at least -130°E to 0°E , with the biggest seasonal differences occurring around -60°E to -80°E longitude. Over the remaining range of longitudes, the December and June densities are more similar, with the June densities sometimes exceeding the December values.

[29] While in each season the RPI and CRRES densities exhibit the same general trends, they differ by more than the uncertainty at high eastern longitudes in the December months and at high western longitudes in the June months. There are a number of possible reasons for this: (i) Because of the orbital configuration, the CRRES June values are

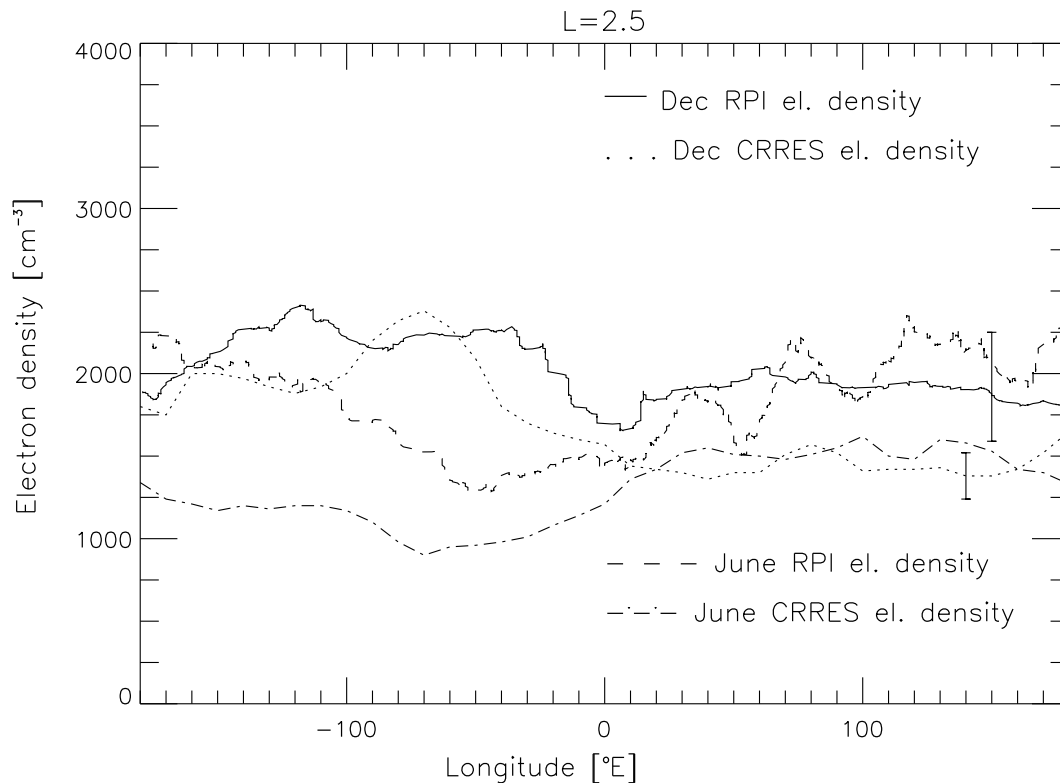


Figure 3. Variation in electron number density with geographic longitude for the June and December months, based on RPI and CRRES observations (from 2001 and 1990–1991, respectively). Error bars represent one standard deviation.

mostly from the 19:00–24:00 MLT sector, and December are values mostly from 3:00–7:00 MLT and 15:00–17:00 MLT, while the RPI data are from the 07:00–16:00 MLT sector; (ii) for CRRES data a wave amplitude-frequency threshold was used to exclude values from outside the plasmasphere, while for RPI data Kp history was used to exclude disturbed intervals; (iii) the CRRES observations actually span $L = 2.5 \pm 0.3$ without adjustment for different L values within this range, while an L^{-4} distribution was assumed for RPI observations; and (iv) actual differences between densities during the CRRES and RPI observation years. Regarding points (ii) and (iv), *Clilverd et al.* [2007] noted that the CRRES data will include some density values when the plasmasphere is refilling following storms. Inspection of the RPI observations shows that for the June and December months there was a tendency for values at high western and eastern longitudes, respectively, to come from days following quiet intervals.

[30] The average RPI electron density over all the June and December months was $1.95 \times 10^3 \text{ cm}^{-3}$. This compares well with the model prediction (based on RPI data) of *Berube et al.* [2005] of $1.93 \times 10^3 \text{ cm}^{-3}$ at $L = 2.5$ for magnetically quiet times.

3.2. Variation in He^+ and Mass Density

[31] The variation in He^+ and ion mass density with geographic longitude for the June and December months is shown in Figure 4, along with the electron densities described above. Note that a log scale has now been used for the ordinate axis. The mass densities, represented by

triangles and squares, include error bars that depict the range between the maximum and minimum densities for each station, averaged across the different analysis methods used. Ion mass densities are in units of $\text{amu} \cdot \text{cm}^{-3}$. The He^+ densities were previously presented and discussed by *Clilverd et al.* [2007, Figure 5] but for clarity here are presented in units of number density.

[32] The He^+ number densities show similar trends with season and longitude as the electron densities. It is clear that there is also a pronounced variation in mass density with longitude between the June and December months, with the mass densities generally tracking but being somewhat higher than the electron densities. This is to be expected because of the effect of heavy ions on the mass density.

[33] In order to investigate these trends in more detail, polynomial curves of best fit were determined for each data set. The R^2 values are respectively 0.17 and 0.10 (for fifth- and sixth-order fits to June and December RPI electron density, respectively), 0.76 and 0.82 (fifth order, June and December He^+ , respectively), and 0.87 and 0.76 (fourth order, June and December mass densities, respectively). These are shown in Figure 5, where the curves have been normalized against the averaged seasonal value. The two solid lines represent the normalized June and December variations in mass density, the dashed lines represent the June and December variations in electron density determined using RPI data, and the dotted lines represent the June and December variations in He^+ density. Also shown, for reference, are the CRRES electron densities averaged with a running mean (dash-dotted lines). It is obvious that each data

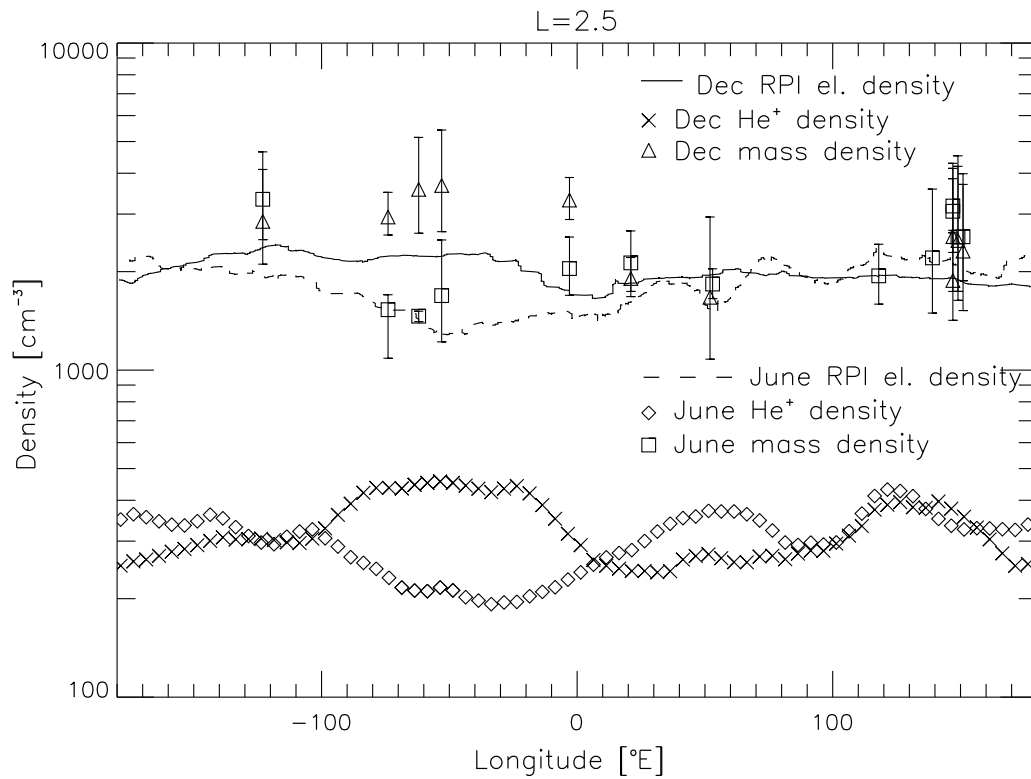


Figure 4. Variations in electron number density, He⁺ density, and ion mass density with geographic longitude for the June and December months. The mass densities, represented by triangles and squares, include error bars representing the range between the maximum and minimum densities for each station averaged across the different analysis methods used.

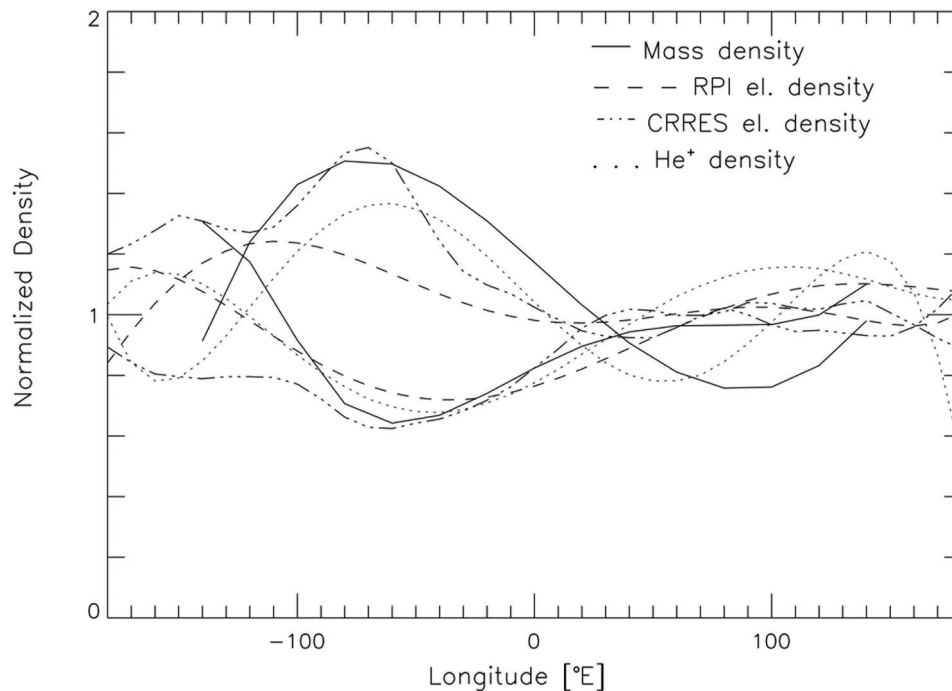


Figure 5. Normalized curves of best fit for electron density (dashed lines, RPI data), He⁺ density (dotted lines), and mass density (solid lines) for the June and December months. See text for further details.

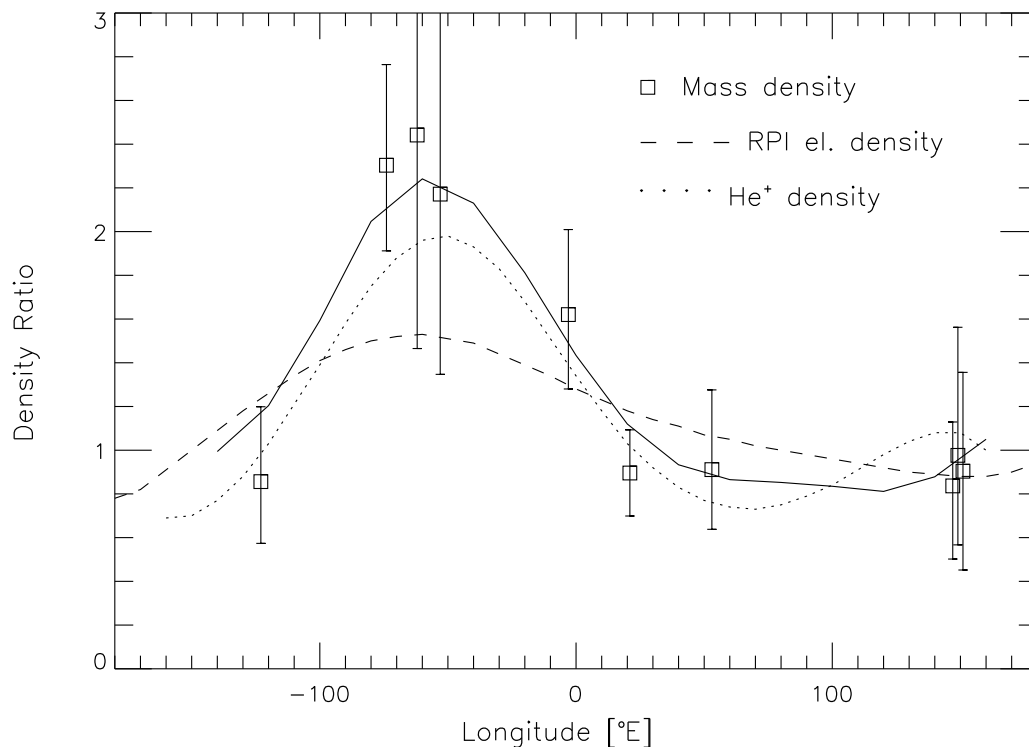


Figure 6. Variation with longitude of the December/June density ratio for electrons (dashed line), He^+ (dotted line), and ion mass density (solid line). Error bars represent the mass density uncertainty for each station and each season.

set exhibits seasonal trends, with the maximum variation between the June and December months occurring around -60°E to -80°E geographic longitude (i.e., east coast of the United States), and almost no variation at 30°E longitude (e.g., European sector).

[34] Finally, Figure 6 shows the variation with longitude of the December/June density ratio in each case. Error bars for the mass density values represent the uncertainty that is due to the range in values for each station and each season (larger error bars mostly relating to single-station data compared with two-station cross-phase measurements), while the curve through these is a fourth-order polynomial fit with $R^2 = 0.96$. It is evident that ion mass density is enhanced by a factor of about 2.2 in the December months compared with the June months near -60°E longitude, but there is no such enhancement beyond -140°E and 30°E longitude. Similarly, He^+ densities are enhanced by a factor of about 2.0 over the same longitude range, while the enhancement in electron density appears to be somewhat lower.

3.3. Variation in Ion Concentration

[35] Ion concentrations were estimated as outlined in section 2.4 for -74°E and -3°E longitude for the June and December months. Results are listed in Table 2, where m is the ion mass loading factor relative to protons and separate columns indicate values derived using CRRES and RPI electron densities. The mass loading factor appears to be somewhat higher at -3° longitude than at -74° longitude and also in the December than in the June months. The former result is consistent with similar findings by *Clilverd*

et al. [2007], who reported a mass loading factor of 2.0 at -10°E compared with 1.3 at -65°E longitude.

4. Discussion

4.1. Determining the Resonant Frequencies

[36] As described in section 2.3, independent manual and automated techniques were used to determine the FLR frequencies. These automated techniques are somewhat more sophisticated than described previously [e.g., *Berube et al.*, 2003] because we allow for examination of single-station or two-station data and because we use pure state and coherence techniques to mask unreliable estimates.

Table 2. Plasma Composition by Season and Longitude

	December (CRRES)	December (RPI)	June (CRRES)	June (RPI)
<i>-74°E Longitude</i>				
Electron density, cm^{-3}	2300	1960	970	1020
Mass loading factor, m	1.28	1.50	1.32	1.25
% H^+ by mass (number)	74 (94)	62 (92)	71 (93)	75 (94)
% He^+ by mass (number)	15 (4.7)	15 (5.5)	18 (5.9)	18 (5.6)
% O^+ by mass (number)	11 (0.9)	24 (1.9)	11 (0.9)	7 (0.6)
<i>-3°E Longitude</i>				
Electron density, cm^{-3}	1600	1766	1200	1564
Mass loading factor, m	2.07	1.88	1.70	1.31
% H^+ by mass (number)	43 (89)	48 (91)	54 (91)	73 (95)
% He^+ by mass (number)	10 (4.9)	10 (4.5)	11 (4.8)	11 (3.7)
% O^+ by mass (number)	48 (6.1)	42 (5.5)	35 (3.7)	16 (1.7)

Comparison showed that the manual and automated methods worked equally well for determining the FLR frequency, except that the latter approach is less labor intensive and facilitates estimates of the statistical significance. One interhemispheric pair (ADL:PTK) was also used in this study.

4.2. Comparison With Previous Observational Studies

[37] Previous studies of the annual variation in electron density were summarized by *Clilverd et al.* [2007, 1991]. The latter study used whistler measurements and showed that at $L = 2.5$ the amplitude of the December/June electron density ratio near -64°E longitude was about 3.0 at solar minimum and about 2.0 at solar maximum. Using CRRES observations, *Clilverd et al.* [2007] found the amplitude of the annual variation at $L = 2.5$ during the 1990 solar maximum was 2.5 at -60°E longitude.

[38] Our observations using RPI electron density data suggest a lower amplitude for the annual variation, of the order of 1.5 for the 2001 solar maximum. The possible reasons for this, outlined in section 3.1, include (i) differences in the local time coverage of the data (19:00–24:00 MLT for CRRES June values; 3:00–7:00 MLT and 15:00–17:00 MLT for CRRES December values; and 7:00–16:00 MLT for RPI data); (ii) differences in how disturbed intervals were excluded and likely inclusion of some poststorm refilling intervals in the CRRES data; (iii) differences in how observations were normalized to $L = 2.5$; and (iv) possible actual differences between the observation years. *Sheeley et al.* [2001, Figure 4] show that the plasmaspheric number density at $L = 3\text{--}4$ is about 1.2 times higher at the local times monitored by CRRES compared with that at the times of the RPI observations. While this might explain some of the difference between the CRRES and RPI data, the day-night variation at $L = 3\text{--}4$ may be exaggerated (relative to $L = 2.5$) by expansion and contraction from the plasma $\mathbf{E} \times \mathbf{B}$ drift.

[39] We found that He^+ and ion mass densities are enhanced by a factor of about 2.0 and 2.2, respectively, in December at $L = 2.5$ near -60°E longitude (Figure 6). The variation of plasmaspheric density has been previously described as a function of L shell, local time, and/or geomagnetic and solar activity [e.g., *Carpenter and Anderson*, 1992; *Craven et al.*, 1997; *Sheeley et al.*, 2001], but we are unaware of any previous descriptions in terms of longitudinal variations (apart from that in the work by *Clilverd et al.*, [2007]). Results from the works by *Newberry et al.* [1989] and *Craven et al.* [1997] indicate that the He^+ density should be about 0.15 that of H^+ under solar maximum conditions. *Fraser et al.* [2005] discussed the significance of heavy ions including O^+ in the plasmasphere and near the plasmopause but with no reference to any systematic variation.

4.3. Implications for Plasmaspheric Models

[40] Empirical models of plasmaspheric electron density have been described by *Carpenter and Anderson* [1992] and *Gallagher et al.* [2000], and a mass density model was presented by *Berube et al.* [2005]. The Carpenter and Anderson plasmasphere model includes a term to represent a December/June ratio at $L \sim 2.5$ of 1.6 (see their equation 3),

but they noted that “proper description of the annual variation may require specification of longitude.”

[41] Our study indicates this further level of specification is important. Furthermore, the annual variation term was carried from the Carpenter and Anderson model into the model by *Gallagher et al.* [2000], who also pointed to the need for further study to establish the importance of this term. In deriving their mass density model, *Berube et al.* [2005] used field line resonance data from a ground magnetometer array located around -71°E to -82°E geographic longitude, i.e., near the peak of the December/June density ratio shown in Figure 5. Therefore, their model represents maximum possible density values in December months, up to 2.5 times higher than over the European and Asian sectors, and should be modified for use at other longitudes.

4.4. Longitudinal Variation in Ion Concentrations

[42] Table 2 summarizes results for December and June ion concentrations calculated for -74°E longitude and -3°E longitude. Since the calculation of ion concentration is based on knowledge of the number density, values using both CRRES and RPI density values are presented. The general trends, however, are the same.

[43] A number of features are evident. First, as expected, the December/June ratio in electron densities is significantly higher at -74°E longitude than at -3°E . However, there appears to be no similar variation in the ratio of December/June mass loading factor m between the two longitudes.

[44] The mass loading factor is clearly larger in both seasons at -3°E longitude than at -74°E . This is a surprising result. Why should plasmaspheric ion concentrations exhibit a longitudinal asymmetry? Inspection of Table 2 shows that this arises mainly from substantially higher O^+ concentrations at -3°E longitude, of the order of 40%–50% by mass (6% by number) in the December months and 20%–35% by mass (2%–4% by number) in the June months, compared with $\sim 7\%$ –20% by mass ($\sim 1\%$ –2% by number) in both seasons at -74°E . In a study of Pc3 eigenfrequencies during July 1983 using longitudinally separated magnetometers at $L = 1.78$, *Sutcliffe et al.* [1987] found that equivalent equatorial H^+ densities were about 60% lower at -10°E geographic longitude than at 20°E . They found that these observations could be explained by the influence of O^+ on eigenfrequencies at low L values and discussed three possible causes: (i) a lower production rate of ionospheric O^+ at the -10°E station that is due to its higher latitude; (ii) a reduction in F region ionization that is due to heating by energetic particle precipitation associated with the South Atlantic anomaly region; and (iii) a decrease in F_2 layer maximum density and height, a decrease in the O^+ scale height immediately above the F_2 peak, and hence a greater loss of O^+ , which is due to the vertical ion drift associated with meridional winds. While these explanations may be appropriate to the low L values discussed by *Sutcliffe et al.*, where field lines have a significant component within the ionosphere, such low-altitude O^+ mass loading effects should be small at $L \sim 2.5$.

[45] It is well established that there is a pronounced annual and longitudinal variation in TEC [*Jee et al.*, 2004; *Mendillo et al.*, 2005]. A detailed consideration of possible reasons for the annual variation in plasmaspheric electron density was presented by *Richards et al.* [2000]. Using the field line

interhemispheric plasma (FLIP) model to calculate the ion densities and electron and ion temperatures along tilted dipole flux tubes, referenced to observed or IRI model ionospheric conditions and topside electron temperature, they were able to reproduce the observed longitudinal variation in electron density at $L = 2.5$. They concluded that the annual variation in plasmaspheric electron density is not caused by a variation in ionospheric density but rather by thermal pressure effects. In the American sector, the extended illumination of the Southern Hemisphere in December causes high electron and ion temperatures in the plasmasphere and topside ionospheres in both hemispheres, maintaining high ionospheric plasma pressure at night and thus high plasmaspheric densities. Conversely, in June, the extended hours of darkness in the Southern Hemisphere create low electron and ion temperatures that lower the ionospheric pressure, allowing the plasmasphere to drain for an extended period. Neutral winds are not expected to play a significant role in the density variation.

[46] Plasmaspheric heavy ion concentrations increase with increasing magnetic activity [e.g., *Berube et al.*, 2005]. This may be due to increased heating of the atmosphere and consequent enhanced upward diffusion of heavy ions [*Yeh and Foster*, 1990] and heating of neutral oxygen in the F region and hence the production of large fluxes of upward moving oxygen ions as a result of precipitation into the atmosphere of energetic O^+ ions [*Torr and Torr*, 1979]. Although our observations are mostly from magnetically quiet times, it is tempting to speculate that the unusually high O^+ concentrations we have found near $-3^\circ E$ longitude, particularly during the December months, may arise from enhanced topside temperatures and hence changes in the O^+ scale height. This might be related to the proximity to the South Atlantic anomaly [*Gledhill*, 1976], but it is not clear if this could account for the amount of heating required. Further investigation of this requires additional Southern Hemisphere magnetometer stations around the longitudes of interest. Results from solar minimum would be of particular interest, since O^+ heating effects may then be expected to be more uniform with longitude.

[47] There are few reports of plasmaspheric ion concentrations in the literature, but the results of *Berube et al.* [2005] suggest maximum possible He^+ and O^+ concentrations (near $-80^\circ E$ longitude) at $L \sim 2.5$ and for quiet times of the order of 36% and 7%, respectively, assuming only one heavy ion species. Our values for these longitudes are of the order of 15%–18% for He^+ and 7%–20% for O^+ . These are comparable to the results of *Berube et al.*, given that we have made no assumption about the ion composition. Our estimated He^+ concentrations (about 5% by number in both seasons and longitudes) and the resultant He^+/H^+ ratio, ~ 0.2 , accord with results found by *Craven et al.* [1997] using in situ observations.

5. Conclusions

[48] We have used ground-based observations of ULF field line eigenoscillations and in situ measurements of electron densities (from the CRRES and IMAGE spacecraft) and He^+ densities (IMAGE) to investigate the annual and longitudinal variations in electron and ion density at $L = 2.5$ in the equatorial plane at solar maximum. We examined the

ULF wave data manually and with new automated algorithms, and we also made use of cross-phase measurements from conjugate stations. We found that near $-60^\circ E$ longitude the electron and ion mass densities are about 1.5 and 2.2 times larger, respectively, in the December months than in the June months. Over the Asia-Pacific region there is little difference between summer and winter densities. Plasmaspheric empirical models will require modification in order to incorporate a longitudinal dependence. By comparing the electron, helium, and mass densities, we also estimated the seasonal variation in H^+ , He^+ , and O^+ concentrations near $-3^\circ E$ longitude and $-74^\circ E$ longitude. In each case the He^+ concentration is about 5% by number, but O^+ concentrations are substantially higher at -3° longitude than at -74° . We speculate that this may be related to enhanced ionospheric temperatures and hence upward fluxes associated with the South Atlantic anomaly.

[49] **Acknowledgments.** We thank Y. Wang and P. Webb for IMAGE/RPI electron density data obtained via the Virtual Wave Observatory, and for magnetometer data we thank the following providers: D. Calp, Geological Survey of Canada (CANMOS); K. Yumoto, Kyushu University, Japan (CPMN); J. Bitterly and M. Bitterly, Ecole et Observatoire des Sciences de la Terre, Strasbourg, France (EOST); accessed via the WDC for Geomagnetism, Kyoto); P. Wilkinson, IPS Radio and Space Services, Sydney (IPS); M. Moldwin, UCLA (MEASURE); PAS; E. Zesta, U. S. Air Force Research Labs, Hanscom AFB, Massachusetts (SAMBA); F. Honary, University of Lancaster, UK (SAMNET), the University of Newcastle (UNC). This work was supported by the Australian Research Council and the University of Newcastle.

[50] Masaki Fujimoto thanks the reviewers for their assistance in evaluating this paper.

References

- Ables, S. T., and B. J. Fraser (2005), Observing the open-closed boundary using cusp-latitude magnetometers, *Geophys. Res. Lett.*, *32*, L10104, doi:10.1029/2005GL022824.
- Bailey, G. J., and R. Sellek (1990), A mathematical model of the Earth's plasmasphere and its application in a study of He^+ at $L = 3$, *Ann. Geophys.*, *8*, 171–190.
- Bailey, G. J., N. Balan, and Y. Z. Su (1997), The Sheffield University plasmasphere ionosphere model—A review, *J. Atmos. Sol. Terr. Phys.*, *59*(13), 1541–1552, doi:10.1016/S1364-6826(96)00155-1.
- Benson, R. F., V. A. Osherovich, J. Fainberg, and B. W. Reinisch (2003), Classification of IMAGE/RPI-stimulated plasma resonances for the accurate determination of magnetospheric electron-density and magnetic field values, *J. Geophys. Res.*, *108*(A5), 1207, doi:10.1029/2002JA009589.
- Benson, R. F., P. A. Webb, J. L. Green, L. Garcia, and B. W. Reinisch (2004), Magnetospheric electron densities inferred from upper-hybrid band emissions, *Geophys. Res. Lett.*, *31*, L20803, doi:10.1029/2004GL020847.
- Berkner, L. V., and H. W. Wells (1938), Non-seasonal change of F_2 -region ion-density, *Terr. Magn. Atmos. Electr.*, *43*(1), 15–36, doi:10.1029/TE043i001p00015.
- Berube, D., M. B. Moldwin, and J. M. Weygand (2003), An automated method for the detection of field line resonance frequencies using ground magnetometer techniques, *J. Geophys. Res.*, *108*(A9), 1348, doi:10.1029/2002JA009737.
- Berube, D., M. B. Moldwin, S. F. Fung, and J. L. Green (2005), A plasmaspheric mass density model and constraints on its heavy ion concentration, *J. Geophys. Res.*, *110*, A04212, doi:10.1029/2004JA010684.
- Berube, D., M. B. Moldwin, and M. Ahn (2006), Computing magnetospheric mass density from field line resonances in a realistic magnetic field geometry, *J. Geophys. Res.*, *111*, A08206, doi:10.1029/2005JA011450.
- Burch, J. L. (2003), The first two years of IMAGE, *Space Sci. Rev.*, *109*, 1–24, doi:10.1023/B:SPAC.0000007510.32068.68.
- Carpenter, D. L. (1962), Electron density variations in the magnetosphere deduced from whistler data, *J. Geophys. Res.*, *67*(9), 3345–3360, doi:10.1029/JZ067i009p03345.
- Carpenter, D. L., and R. R. Anderson (1992), An ISEE/whistler model of equatorial electron density in the magnetosphere, *J. Geophys. Res.*, *97*(A2), 1097–1108, doi:10.1029/91JA01548.

- Carpenter, D. L., and C. G. Park (1973), On what ionospheric workers should know about the plasmopause-plasmasphere, *Rev. Geophys.*, *11*(1), 133–154, doi:10.1029/RG011i001p00133.
- Chappell, C. R., K. K. Harris, and G. W. Sharp (1970), The morphology of the bulge region of the plasmasphere, *J. Geophys. Res.*, *75*(19), 3848–3861, doi:10.1029/JA075i019p03848.
- Clilverd, M. A., A. J. Smith, and N. R. Thomson (1991), The annual variation in quiet time plasmaspheric electron density determined from whistler mode group delays, *Planet. Space Sci.*, *39*, 1059–1067, doi:10.1016/0032-0633(91)90113-0.
- Clilverd, M. A., et al. (2003), In situ and ground-based intercalibration measurements of plasma density at $L = 2.5$, *J. Geophys. Res.*, *108*(A10), 1365, doi:10.1029/2003JA009866.
- Clilverd, M. A., N. P. Meredith, R. B. Horne, S. A. Glauert, R. R. Anderson, N. R. Thomson, F. W. Menk, and B. R. Sandel (2007), Longitudinal and seasonal variations in plasmaspheric electron density: Implications for electron precipitation, *J. Geophys. Res.*, *112*, A11210, doi:10.1029/2007JA012416.
- Craven, P. D., D. L. Gallagher, and R. H. Comfort (1997), Relative concentration of He⁺ in the inner magnetosphere as observed by the DE 1 retarding ion mass spectrometer, *J. Geophys. Res.*, *102*(A2), 2279–2289, doi:10.1029/96JA02176.
- Denton, R. E., et al. (2009), Field line distribution of density at $L=4.8$ inferred from observations by CLUSTER, *Ann. Geophys.*, *27*, 705–724, doi:10.5194/angeo-27-705-2009.
- Fraser, B. J., J. L. Horwitz, J. A. Slavin, Z. C. Dent, and I. R. Mann (2005), Heavy ion mass loading of the geomagnetic field near the plasmopause and ULF wave implications, *Geophys. Res. Lett.*, *32*, L04102, doi:10.1029/2004GL021315.
- Gallagher, D. L., P. D. Craven, and R. H. Comfort (2000), Global core plasma model, *J. Geophys. Res.*, *105*(A8), 18,819–18,833, doi:10.1029/1999JA000241.
- Gallagher, D. L., M. L. Adrian, and M. W. Liemohn (2005), Origin and evolution of deep plasmaspheric notches, *J. Geophys. Res.*, *110*, A09201, doi:10.1029/2004JA010906.
- Gledhill, J. A. (1976), Aeronomic effects of the South Atlantic Anomaly, *Rev. Geophys.*, *14*(2), 173–187, doi:10.1029/RG014i002p00173.
- Goldstein, J., M. Spasojević, P. H. Reiff, B. R. Sandel, T. Forrester, D. L. Gallagher, and B. W. Reinisch (2003), Identifying the plasmopause in IMAGE EUV data using IMAGE RPI in situ steep density gradients, *J. Geophys. Res.*, *108*(A4), 1147, doi:10.1029/2002JA009475.
- Grew, R. S., F. W. Menk, M. A. Clilverd, and B. R. Sandel (2007), Mass and electron densities in the inner magnetosphere during a prolonged disturbed interval, *Geophys. Res. Lett.*, *34*, L02108, doi:10.1029/2006GL028254.
- Güter, S. M., C. E. Rasmussen, T. I. Gombosi, J. J. Sojka, and R. W. Schunk (1995), What is the source of observed annual variations in plasmaspheric density?, *J. Geophys. Res.*, *100*(A5), 8013–8020, doi:10.1029/94JA02866.
- Hattingh, S. K. F., and P. R. Sutcliffe (1987), Pc 3 Pulsation eigenperiod determination at low latitudes, *J. Geophys. Res.*, *92*(A11), 12,433–12,436, doi:10.1029/JA092iA11p12433.
- Jee, G., R. W. Schunk, and L. Scherliess (2004), Analysis of TEC data from the TOPEX/Poseidon mission, *J. Geophys. Res.*, *109*, A01301, doi:10.1029/2003JA010058.
- Kawamura, S., N. Balan, Y. Otsuka, and S. Fukao (2002), Annual and semiannual variations of the midlatitude ionosphere under low solar activity, *J. Geophys. Res.*, *107*(A8), 1166, doi:10.1029/2001JA000267.
- King, J. W., G. L. Hawkins, and C. Seabrook (1968), The seasonal behaviour of the topside ionosphere, *J. Atmos. Terr. Phys.*, *30*, 1701–1706, doi:10.1016/0021-9169(68)90018-4.
- Kutiev, I. S., P. G. Marinov, and S. Watanabe (2006), Model of topside ionosphere scale height based on topside sounder data, *Adv. Space Res.*, *37*, 943–950, doi:10.1016/j.asr.2005.11.021.
- Mendillo, M., C.-L. Huang, X. Pi, H. Rishbeth, and R. Meier (2005), The global ionospheric asymmetry in total electron content, *J. Atmos. Sol. Terr. Phys.*, *67*, 1377–1387, doi:10.1016/j.jastp.2005.06.021.
- Menk, F. W., D. Orr, M. A. Clilverd, A. J. Smith, C. L. Waters, D. Milling, and B. J. Fraser (1999), Monitoring spatial and temporal variations in the dayside plasmasphere using geomagnetic field line resonances, *J. Geophys. Res.*, *104*(A9), 19,955–19,969, doi:10.1029/1999JA900205.
- Menk, F., C. Waters, and B. Fraser (2000), Field line resonances and waveguide modes at low latitudes: 1. Observations, *J. Geophys. Res.*, *105*(A4), 7747–7761, doi:10.1029/1999JA900268.
- Menk, F. W., I. R. Mann, A. J. Smith, C. L. Waters, M. A. Clilverd, and D. K. Milling (2004), Monitoring the plasmopause using geomagnetic field line resonances, *J. Geophys. Res.*, *109*, A04216, doi:10.1029/2003JA010097.
- Menk, F. W., M. A. Clilverd, K. H. Yearby, G. Milneviski, N. R. Thomson, and M. C. Rose (2006), ULF Doppler oscillations of $L = 2.5$ flux tubes, *J. Geophys. Res.*, *111*, A07205, doi:10.1029/2005JA011192.
- Newberry, I. T., R. H. Comfort, P. G. Richards, and C. R. Chappell (1989), Thermal He in the plasmasphere: Comparison of observations with numerical calculations, *J. Geophys. Res.*, *94*(A11), 15,265–15,276, doi:10.1029/JA094iA11p15265.
- Park, C. G., D. L. Carpenter, and D. B. Wiggin (1978), Electron density in the plasmasphere: Whistler data on solar cycle, annual and diurnal variations, *J. Geophys. Res.*, *83*(A7), 3137–3144, doi:10.1029/JA083iA07p03137.
- Pilipenko, V., K. Yumoto, E. Federov, and N. Yagova (1999), Hydromagnetic spectroscopy of the magnetosphere with Pc3 geomagnetic pulsations along the 210° meridian, *Ann. Geophys.*, *17*, 53–65.
- Reinisch, B. W., et al. (2001), First results from the Radio Plasma Imager on IMAGE, *Geophys. Res. Lett.*, *28*(6), 1167–1170, doi:10.1029/2000GL012398.
- Richards, P. G., T. Chang, and R. H. Comfort (2000), On the causes of the annual variation in the plasmaspheric electron density, *J. Atmos. Sol. Terr. Phys.*, *62*, 935–946, doi:10.1016/S1364-6826(00)00039-0.
- Rippeth, Y., R. J. Moffett, and G. J. Bailey (1991), Model plasmasphere calculations for L -values near 2.5 at the longitude of Argentine Islands, Antarctica, *J. Atmos. Terr. Phys.*, *53*(6–7), 551–555, doi:10.1016/0021-9169(91)90082-1.
- Rishbeth, H., and I. C. F. Müller-Wodarg (2006), Why is there more ionosphere in January than in July? The annual asymmetry in the F2-layer, *Ann. Geophys.*, *24*, 3293–3311, doi:10.5194/angeo-24-3293-2006.
- Sandel, B. R., R. A. King, W. T. Forrester, D. L. Gallagher, A. L. Broadfoot, and C. C. Curtis (2001), Initial results from the IMAGE extreme ultraviolet imager, *Geophys. Res. Lett.*, *28*(8), 1439–1442, doi:10.1029/2001GL012885.
- Sandel, B. R., J. Goldstein, D. L. Gallagher, and M. Spasojević (2003), Extreme ultraviolet imager observations of the structure and dynamics of the plasmasphere, *Space Sci. Rev.*, *109*, 25–46, doi:10.1023/B:SPAC.0000007511.47727.5b.
- Seaton, S. L., and L. V. Berkner (1939), Non-seasonal behavior of the F-region, *Terr. Magn. Atmos. Electr.*, *44*(3), 313–319, doi:10.1029/TE044i003p00313.
- Sheeley, B. W., M. B. Moldwin, H. K. Rassoul, and R. R. Anderson (2001), An empirical plasmasphere and rough density model: CRRES observations, *J. Geophys. Res.*, *106*(A11), 25,631–25,641, doi:10.1029/2000JA000286.
- Smith, R. L. (1961), Electron densities in the outer ionosphere deduced from nose whistlers, *J. Geophys. Res.*, *66*(8), 2578–2579, doi:10.1029/JZ066i008p02578.
- Su, Y. Z., G. J. Bailey, and K.-I. Oyama (1998), Annual and seasonal variations in the low-latitude topside ionosphere, *Ann. Geophys.*, *16*, 974–985, doi:10.1007/s00585-998-0974-0.
- Sutcliffe, P. R., S. K. F. Hattingh, and H. F. V. Boshoff (1987), Longitudinal effects on the eigenfrequencies of low-latitude Pc 3 pulsations, *J. Geophys. Res.*, *92*(A3), 2535–2543, doi:10.1029/JA092iA03p02535.
- Tarcsai, G., P. Szemerédy, and L. Hegymegi (1988), Average electron density profiles in the plasmasphere between $L = 1.4$ and 3.2 deduced from whistlers, *J. Atmos. Terr. Phys.*, *50*, 607–611, doi:10.1016/0021-9169(88)90058-X.
- Taylor, J. P. H., and A. D. M. Walker (1984), Accurate approximate formulae for toroidal mode standing hydromagnetic oscillations in a dipolar geomagnetic field, *Planet. Space Sci.*, *32*, 1119–1124, doi:10.1016/0032-0633(84)90138-7.
- Titheridge, J. E., and M. J. Buonsanto (1983), Annual variations in the electron content and height of the F layer in the northern and southern hemispheres, related to neutral composition, *J. Atmos. Terr. Phys.*, *45*(10), 683–696, doi:10.1016/S0021-9169(83)80027-0.
- Torr, M. R., and D. G. Torr (1973), The seasonal behaviour of the F2-layer of the ionosphere, *J. Atmos. Terr. Phys.*, *35*, 2237–2251, doi:10.1016/0021-9169(73)90140-2.
- Torr, M. R., and D. G. Torr (1979), Energetic oxygen: A direct coupling mechanism between the magnetosphere and thermosphere, *Geophys. Res. Lett.*, *6*(9), 700–702, doi:10.1029/GL006i009p00700.
- Tremellen, K. W., and J. W. Cox (1947), The influence of wave-propagation on the planning of short-wave communication, *Proc. Inst. Electr. Eng.*, *94*, 200–219.
- Vellante, M., and M. Förster (2006), Inference of the magnetospheric plasma mass density from field line resonances: A test using a plasmasphere model, *J. Geophys. Res.*, *111*, A11204, doi:10.1029/2005JA011588.
- Vellante, M., U. Villante, M. De Lauretis, R. Core, A. Best, D. Lenner, and V. A. Pilipenko (1993), Simultaneous geomagnetic pulsation observations at two latitudes: Resonant mode characteristics, *Ann. Geophys.*, *11*, 734–741.

- Walker, A. D. M., J. M. Ruohoniemi, K. B. Baker, R. A. Greenwald, and J. C. Samson (1992), Spatial and temporal behaviour of ULF pulsations observed by the Goose Bay HF radar, *J. Geophys. Res.*, *97*(A8), 12,187–12,202, doi:10.1029/92JA00329.
- Waters, C. L., F. W. Menk, and B. J. Fraser (1994), Low latitude geomagnetic field line resonance: Experiment and modeling, *J. Geophys. Res.*, *99*(A9), 17,547–17,558, doi:10.1029/94JA00252.
- Yeh, H.-C., and J. C. Foster (1990), Storm time heavy ion outflow at mid-latitude, *J. Geophys. Res.*, *95*(A6), 7881–7891, doi:10.1029/JA095iA06p07881.
- Yonezawa, T. (1971), The solar-activity and latitudinal characteristics of the seasonal, non-seasonal and semi-annual variations in the peak electron densities of the F2-layer at noon and at midnight in middle and low latitudes, *J. Atmos. Terr. Phys.*, *33*, 889–907, doi:10.1016/0021-9169(71)90089-4.
- Yonezawa, T., and Y. Arima (1959), On the seasonal and non-seasonal annual variations and the semi-annual variation in the noon and midnight electron densities of the F2 layer in middle latitudes, *J. Radio Res. Lab. Jpn.*, *6*, 293–309.
- Zou, L., H. Rishbeth, I. C. F. Müller-Wodarg, A. D. Aylward, G. H. Millward, T. J. Fuller-Rowell, D. W. Idenden, and R. J. Moffett (2000), Annual and semiannual variations in the ionospheric F2-layer: I. Modeling, *Ann. Geophys.*, *18*, 927–944, doi:10.1007/s00585-000-0927-8.
-
- S. T. Ables, R. S. Grew, and F. W. Menk, School of Mathematical and Physical Sciences, University of Newcastle, University Drive, Newcastle, NSW 2308, Australia. (fred.menk@newcastle.edu.au)
- M. A. Clilverd, British Antarctic Survey, Madingley Road, Cambridge CB3 0ET, UK.
- B. R. Sandel, Lunar and Planetary Laboratory, University of Arizona, 1629 E. University Blvd., Tucson, AZ 85721-0092, USA.